Available online at www.sciencedirect.com

ScienceDirect

Procedia Structural Integrity 3 (2017) 450–458

Structural Integrity Procedia

www.elsevier.com/locate/procedia

XXIV Italian Group of Fracture Conference, 1-3 March 2017, Urbino, Italy

An investigation on the "width and size effect" in the evaluation of the fracture energy of concrete

Christian Carloni[a], Mattia Santandrea[a]*, Roman Wendner[b]

[a]*University of Bologna-DICAM, Viale Risorgimento 2, Bologna 40136, Italy*
[b]*University of Natural Resources and Life Sciences-Christian Doppler Laboratory LICROFAST, Peter-Jordan-Straße 82, Wien 1190, Austria*

Abstract

The parameters that describe the fracture behavior of concrete are crucial to investigate numerically the response of reinforced concrete (RC) structures. Among them, the fracture energy plays a key role in all those applications that aim to simulate the behavior of RC structures. The fracture energy is a characteristic property of a material but its experimental evaluation could be difficult for quasi-brittle materials such as concrete due to the "width effect" and "size effect" that can lead to some uncertainties in the definition of this parameter. This study presents the results of an experimental campaign conducted on notched specimens to evaluate the fracture energy of concrete. Concrete prisms with different sizes were tested using a three-point bending (TPB) set-up to evaluate the influence of the width and the size on the results. The setup has been designed to become potentially part of the ACI 446 report on fracture. Digital image correlation (DIC) was used to qualitatively and quantitatively study the strain field near the crack tip. Preliminary numerical simulations were performed to investigate the "width effect" in a discrete element framework.

Peer-review under responsibility of the Scientific Committee of IGF Ex-Co.

Keywords: Fracture mechanics; concrete; fracture energy; width effect; size effect.

1. Introduction

The tensile strength and the fracture parameters of concrete are important properties of concrete when the anchorage of deformed bars, shear forces in slabs and beams, splitting under concentrated forces, unreinforced pipes, and bond of composite materials (Carloni, 2014) are investigated. Although the influence of these properties on the behavior of

* Corresponding author. Tel.: +39 051 20 9 3375.
E-mail address: mattia.santandrea3@unibo.it

Copyright © 2017 The Authors. Published by Elsevier B.V. This is an open access article under the CC BY-NC-ND license (http://creativecommons.org/licenses/by-nc-nd/4.0/).
Peer-review under responsibility of the Scientific Committee of IGF Ex-Co.
10.1016/j.prostr.2017.04.065

concrete elements is well known, they have been rarely used in design codes. For example, in many European codes the definition of the shear strength of concrete elements is based on empirical design formulas, neglecting any fracture parameters in these formulations. Fortunately, due to the increasing interest on the fracture mechanics of concrete in the last few decades and the pioneering work of some researchers (Bažant, 1997), some fracture parameters have been considered for design formulas. For example, the definition of the load-carrying capacity of composite strips bonded to concrete (Carloni, 2014) depends on the fracture properties of the interface.

The main fracture parameter of concrete is the fracture energy G_F, i.e. the energy required to create and fully break the elementary unit area of a cohesive crack. It is well known that the classical linear elastic fracture mechanics (LEFM) of sharp cracks is inadequate for concrete structures, as pointed out first by Kesler et al. (1972). This conclusion was confirmed by Walsh et al. (1976), who conducted an experimental campaign on geometrically similar notched beams of different sizes. Plotting the results in a double logarithmic diagram of nominal strength versus size they observed that the diagram deviates from a straight line of slope -1/2 predicted by LEFM. The inapplicability of LEFM to concrete is due to the development of a sizable nonlinear zone that develops at the fracture front. In concrete and other quasi-brittle materials, the nonlinear zone is almost entirely filled by the fracture process zone (FPZ) that is defined as the zone in which the material undergoes softening damage, while the plastic flow is next to nonexistent. In addition, the length of the FPZ, which is equal or proportional to the so-called characteristic length (Hillerborg, 1985), l_{ch}, may occupy a larger portion of the cross-section of the structural member or encompass the whole cross-section. Due to the high influence of the concrete element dimensions on the crack propagation and on fracture parameters, the "size and width effects" have gained a terrific interest in the evaluation of the fracture energy of concrete. Fracture mechanics of quasi brittle materials was studied also through numerical analysis. New approaches to the modelling of quasi-brittle fracture, as the lattice model, have been developed, proposing as an alternative to traditional nonlinear analysis as the cohesive crack model proposed by Hillerborg (1976) and by Petterson (1981) or the crack band model proposed by Bažant (1983).

This study presents the results of an experimental campaign conducted on notched specimens to evaluate the fracture energy of concrete. Concrete prisms with different sizes were tested using a three-point bending (TPB) set-up to evaluate the influence of the width and the size of the prisms on the results. The set-up has been designed to become potentially part of the ACI 446 report on fracture. Digital image correlation (DIC) was used to qualitatively and quantitatively study the strain field near the crack tip. Preliminary numerical simulations were performed to investigate the "width effect" and to confirm experimental results.

2. Experimental Program

2.1. Materials

All concrete prisms were cast from the same batch of concrete. The concrete was normalweight with portland cement and a maximum aggregate size of 15 mm. Compressive and tensile strength of concrete were measured at different ages. Compressive strength was determined using 150 mm side cubes and 150 mm × 300 mm cylinders that were tested according to EN 12390-3 (2009). Tensile strength was determined using 150 mm × 300 mm cylinders that were tested according to EN 12390-6 (2009). The average values of three tests for each age are plotted in Figure 1.

Fracture mechanics tests were performed approximatively 300 days after prisms were cast. The behavior of the cubic compressive strength at different ages was fitted using the formula proposed in Eurocode 2 (2004):

$$R_{cm}(t) = \exp\left\{ s\left[1 - \left(\frac{28}{t} \right)^{1/2} \right] \right\} R_{cm} \tag{1}$$

where R_{cm} is the mean cubic compressive strength at 28 days obtained from experimental tests, while s is a parameter defined through a non-linear regression. The coefficient s was found to be equal to 0.31, which is slightly higher than prescriptions suggested in Eurocode 2 (2004). The same formula was used to fit the results of tensile tests, using the mean tensile strength at 28 days obtained from splitting tests, f_{tm}, instead of R_{cm} (coefficient s equal to 0.15). Since the

compressive tests on cylinders were not performed until the age of 84 days, the cylinder compressive strength over time behavior was obtained by scaling the curve from cubes in order to best fit the experimental data of cylinders. The compressive strength of cubes and cylinders and the tensile strength at 300 days evaluated from the fitting of experimental data is equal to 30.78 MPa, 26.83 MPa, and 2.56 MPa respectively.

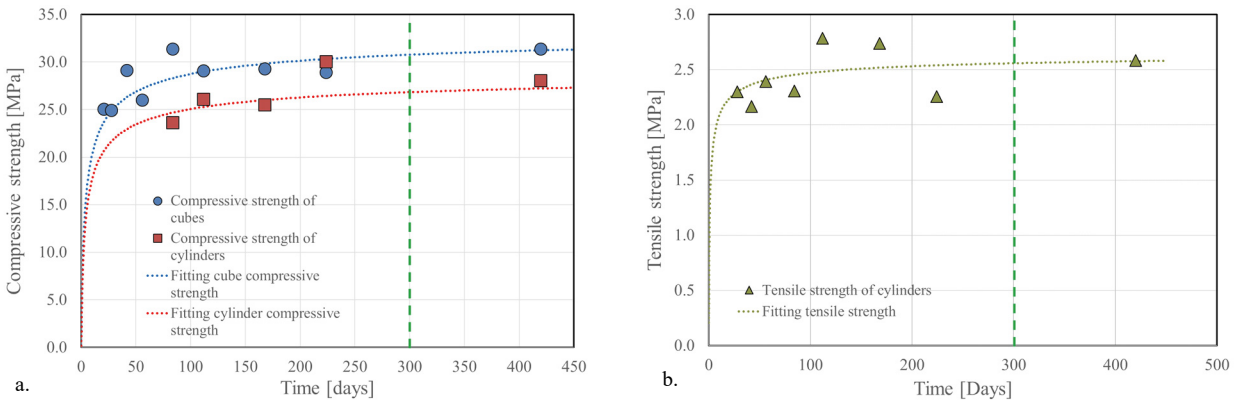

Fig. 1. Compressive (a) and tensile strength (b) of concrete as a function of time.

2.2. Test set-up

Twelve concrete prisms with different widths, depths, and lengths were tested using a TPB set-up (Figure 2) in order to investigate the role of the width and size effects in the evaluation of the fracture mechanics parameters. Specimens were named following the notation FM_X_Y_W_A_Z, where X indicates the specimen depth (d) in mm, Y represents the specimen width (b) in mm, W indicates the specimen free span (S) in mm, A denotes the use of DIC (D = DIC was used, ND = DIC was not used), and Z = specimen number.

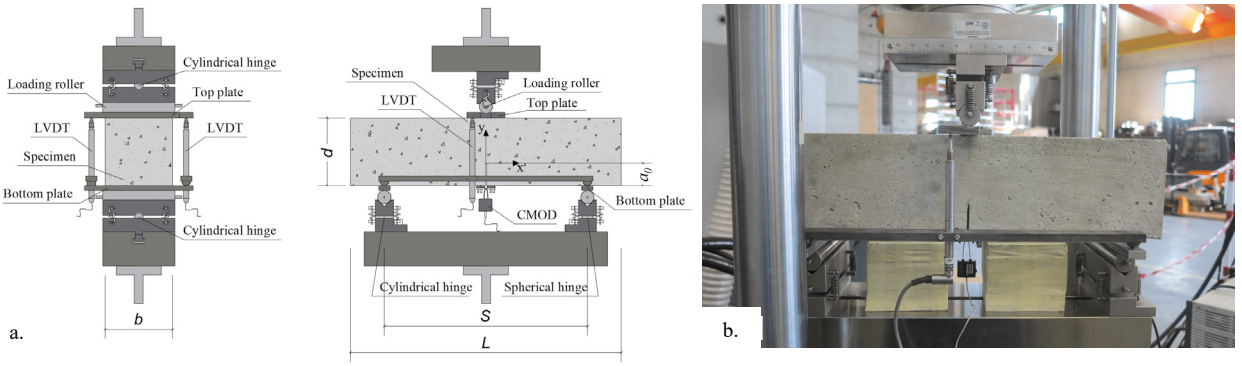

Fig. 2. Fracture mechanics set-up: sketch (a) and photograph (b).

The dimensions of all concrete prisms obtained as the average of three measurements are presented in Table 1. All concrete prisms had a central notch with a V-shaped tip. The notch length a_0 was equal to one third of the prism depth D. The net span S was equal to three times the depth of the specimen. The loading apparatus consisted of two bottom cylindrical rollers that supported the prism base and a cylindrical roller at the top of the specimen, centered with respect to its length that was used to apply the load. Two steel plates were glued to the bottom face of the specimen and placed on the support rollers to reduce friction. An “S-shaped” steel plate with a central V-shaped section was glued to the top face of the specimen to rest firmly the loading cylindrical roller. Both the top and the bottom plates had a length exceeding the prism width. On both sides of the concrete prism, a steel element, with a semi-spherical and a cylindrical support rested on the bottom plates. Each steel element fastened a linear variable displacement

transducer (LVDT) that reacted off of the "S-shaped" top plate. The two LVDTs measured the vertical displacement δ of the prism where the load was applied. Two small steel plates were glued to the bottom face of the prism near each edge of the central notch. Two screws were welded on each small plate in order to fix the knives that provided the fastening of a clip-on gage. The clip-on gage measured the crack mouth opening displacement (CMOD) and was used to control the test. The rate of the test was equal to 0.001 mm/s. The set-up herein presented has been designed to become potentially part of the ACI 446 report on fracture. Rates higher than 0.001 mm/s were considered in preliminary tests but disregarded because the peak load was reached within seconds from the beginning of the test.

Table 1. Specimens dimensions.

Specimen	Depth (*mm*)	Width (*mm*)	Length (*mm*)	Span (*mm*)	Weight (*N*)	Notch (*mm*)
FM_75_75_210_D_1	75.7	72.7	296.8	210	35.1	25.0
FM_75_75_210_D_2	75.5	76.0	296.3	210	36.5	23.0
FM_75_75_210_ND_3	75.2	76.8	297.0	210	36.8	23.0
FM_75_150_210_D_1	74.8	153.6	299.9	210	76.6	25.0
FM_75_150_210_D_2	76.0	152.7	296.3	210	76.0	26.0
FM_75_150_210_D_3	75.3	153.6	297.0	210	74.9	24.0
FM_150_75_450_ND_1	152.8	75.0	599.3	450	153.6	50.0
FM_150_75_450_D_2	152.8	75.7	599.0	450	151.0	51.5
FM_150_75_450_D_3	153.2	77.2	599.5	450	156.4	51.0
FM_150_150_450_ND_1	149.8	152.7	599.3	450	306.3	53.5
FM_150_150_450_D_2	149.7	152.8	598.8	450	301.9	55.0
FM_150_150_450_D_3	149.7	152.8	599.3	450	303.9	50.5

3. Test result

In this section, the experimental results are presented. Twelve fracture mechanics tests were performed using a TPB set-up. Two different widths and two different depths of the concrete prisms were considered. Figure 3 shows the load per unit width, *P/b*, plotted versus CMOD (Figure 3a) and displacement δ (Figure 3b) for 75 mm depth specimens.

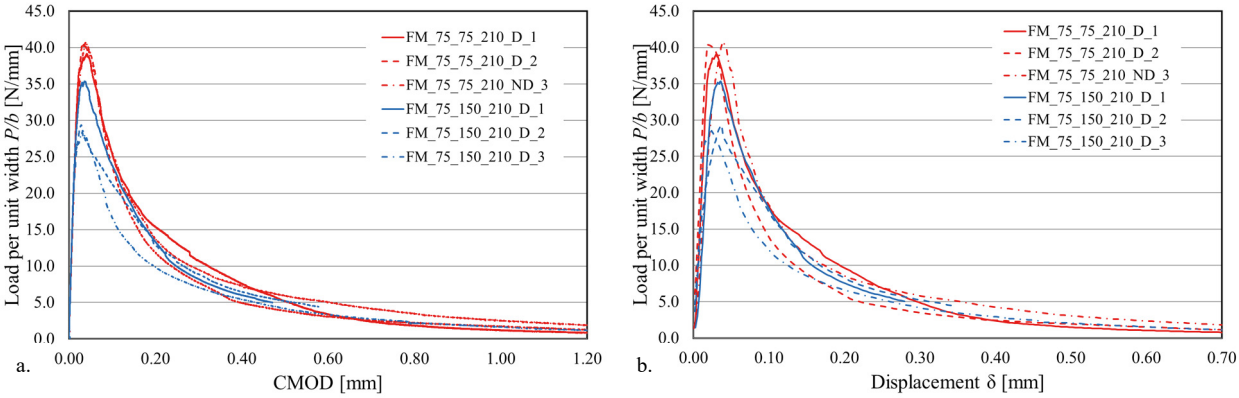

Fig. 3. Load per unit width vs. CMOD (a) and load per unit width vs. displacement (b) for 75 mm depth specimens.

All load responses exhibit a similar trend. Concrete notched specimens show an initial linear branch, followed by a non-linear portion until the peak load is reached. At peak load, the maximum tensile strength of concrete is reached near the crack tip and part of the FPZ has formed (Elices et al. 1996). Crack propagation occurs after the peak in the

descending branch of the load response, which is characterized by a long tail until the specimen finally breaks at a value of the load close to zero. Few specimens failed prematurely at a value of the load approximately equal to 15% of the peak load, therefore the tail of the response was incomplete. In those specimens, the fracture surface was similar to those that exhibited a long tail. A typical cohesive crack pattern of a specimen tested (FM_75_150_210_D_2) and the relative crack surfaces are shown in Figure 4a and b, respectively.

a. 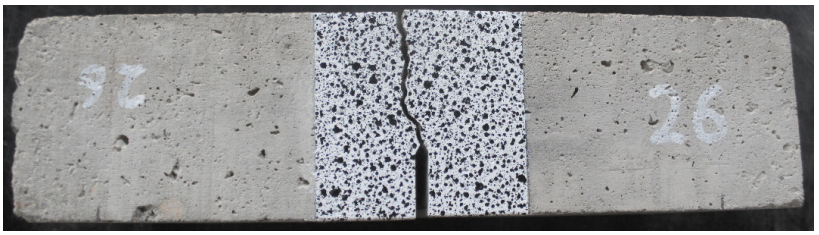 b. 

Fig. 4. Specimen FM_75_150_210_D_2 at failure: side view (a) and surfaces of the fracture (b).

4. Evaluation of the fracture energy

The fracture energy, G_F, of concrete was evaluated from the area under the load-deflection response as proposed by Hillerborg (1985) and Elices et al. (1992). The value of G_F was adjusted to include the work done by the self-weight, P_0, of the specimen, as showed in Figure 5a. The value of G_F for each specimen is reported in Table 2. It can be observed that the values of the fracture energy, independently of the width or the depth of the specimen, are similar. These results would suggest that the fracture energy, G_F, is almost size and width-independent, therefore it can be considered a material property. In order to verify the accuracy in the evaluation of P_0, it is possible to compare the analytical and experimental values of the vertical displacement due to the self-weight at midspan. The self-weight, P_0, is considered as a concentrated load (Gerstle, 2010), and is obtained comparing the bending moment due to a distributed load with the one due to a concentrated load:

$$\frac{mgLS}{4}-\frac{mgL^2}{8}=\frac{P_0 S}{4}\rightarrow P_0=mg\left(1-\frac{L}{2S}\right) \tag{2}$$

Where m is the mass of the specimen and g is the acceleration of gravity.

The analytical displacement due to the self-weight can be evaluated through the following fracture mechanics formulas:

$$u=\frac{P_0}{bE}\hat{v}(\alpha) \qquad \hat{v}(\alpha)=\hat{v}_0+\hat{v}^c(\alpha) \qquad v_0=u_0\frac{bE}{P_0} \qquad \hat{v}^c(\alpha)=2\int_0^{\alpha}\hat{k}^2(\alpha')d\alpha' \tag{3, a-b-c-d}$$

in which E is the elastic modulus of concrete evaluated according to Eurocode 2 (2004), u_0 is the elastic displacement of the structure in the absence of a crack, k is the stress intensity factor, and α is equal to a_0/d. The displacement due to the self-weight of the specimen can be obtained from the experimental response. If the initial pseudo linear response is extended toward the quadrant of negative values of the displacement, the intersection of the linear response with the horizontal line corresponding to $-P_0$ would provide an estimate of the deflection due to the selfweight. The values of the initial displacement due to the self-weight were reported in Table 2 for both the analytical and experimental procedures. No significant difference is observed between the theoretical and the experimental values of the

displacement, which suggests that LEFM formulas could be employed for this calculation.

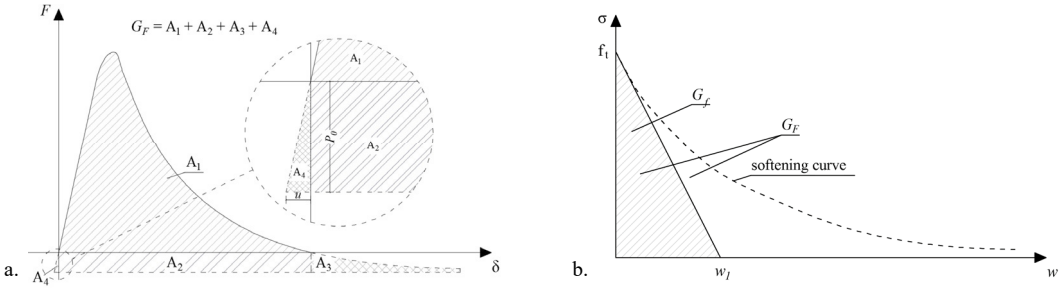

Fig. 5. Evaluation of the fracture energies G_F (a) and G_f (b).

Table 2. Fracture mechanics results.

Specimen	G_F (*N/mm*)		G_f (*N/mm*)		u_{theor} (μm)	u_{exp} (μm)	u_{theor}/ u_{exp} (%)	σ_N (MPa)
FM_75_75_210_D_1	0.112	0.109 (CoV 0.12)	0.081	0.074 (CoV 0.10)	0.088	0.067	130%	2.15
FM_75_75_210_D_2	0.095		0.067		0.074	0.060	123%	2.24
FM_75_75_210_ND_3	0.121		0.075		0.074	0.098	76%	2.27
FM_75_150_210_D_1	0.109	0.102 (CoV 0.10)	0.056	0.032 (CoV 0.66)	0.092	0.081	114%	1.99
FM_75_150_210_D_2	0.107		0.023		0.098	0.097	102%	1.60
FM_75_150_210_D_3	0.090		0.017		0.082	0.081	102%	1.59
FM_150_75_450_ND_1	0.125	0.127 (CoV 0.12)	/	0.072 (CoV 0.38)	0.455	0.693	66%	2.14
FM_150_75_450_D_2	0.143		0.092		0.476	0.752	63%	1.88
FM_150_75_450_D_3	0.112		0.053		0.467	0.640	73%	1.69
FM_150_150_450_ND_1	0.099	0.104 (CoV 0.05)	0.072	0.059 (CoV 0.26)	0.569	0.603	94%	1.69
FM_150_150_450_D_2	0.109		0.064		0.605	0.750	81%	1.60
FM_150_150_450_D_3	0.102		0.042		0.490	0.779	63%	1.59

Another fracture energy, G_f, corresponding to the area under the initial tangent of the softening curve σ-*w* (Figure 5b), can be evaluated using the tensile strength of concrete and the peak load, as described by Gerstle (2010). As noticed by Planas et al. (1992), it is solely G_f that controls the maximum loads of structures and thus the size effect. The values of G_f are reported in Table 2. If specimens with the same depth are considered, it can be noted that the value of G_f is affected by the width of the specimen. For a depth of 75 mm, the average value of G_f is equal to 0.032 N/mm or to 0.074 N/mm, for 150 mm width specimens and 75 mm width specimens, respectively. A similar trend was obtained for 150 mm depth specimens. The width effect is confirmed by comparing the load per unit width responses of Figure 3, where the peak load appears usually higher for specimens with a smaller width. Results in Table 2 highlight also a size-effect. Squared cross-section specimens 75 mm x 75 mm and 150 mm x 150 mm have G_f equal to 0.074 N/mm and 0.059 N/mm, respectively. At the same time, for specimens with the same width but different depth, it can be observed that an increase in the depth causes a decrease in the nominal stress, σ_N, (Bažant , 1997) at peak. The width effect has several causes that can be summarized as follows:

- Changes in the width of the specimens can be associated with a shifting from a plane stress condition (thin specimen) to a plane strain state (thick specimen) affecting therefore the peak load.
- Wall effect: during casting, large aggregates tend to distribute in the central portion of the mold, with a lower concentration near the edges. The concrete near the edges is usually rich of mortar and it has slightly different properties with respect to the concrete in the core of the prism. This aspect is emphasized for thin specimens.

- For thick specimens, the cure of the concrete take usually long time, especially in the core of the specimen. This aspect can lead to erroneous result if the specimens are tested too early with respect to the casting date. Specimens were tested at 300 days of age so curing of specimens should not be an issue in the experimental results herein presented. This is should have not influenced the results of the current study.
- Since concrete is a heterogeneous material, for larger specimens is easier to find a weak portion of concrete with respect to a thin specimen.

5. Digital image correlation (DIC) analysis

In this section, digital image correlation (DIC) was used to evaluate the strain field near the crack tip. Displacements and strains were obtained for different square areas (subsets) for a 5 pixel step size, which provided points spaced at approximately 0.75 mm. A subset size of 41 pixels (approximately 6.30 mm) edge was employed. The DIC analysis reported in this section refers to the Cartesian system shown in Figure 2. Figure 6 shows the strain component ε_{xx} in the central portion of the prism for specimen FM_75_150_210_D_2. The strain profile along the crack ligament for different values of the load is reported in Figure 6a. It can be observed that at peak load (point C) part of the FPZ has formed, and near the crack tip strains have exceeded the ultimate tensile strain of concrete, ε_t, equal to 0.00009, which was obtained by dividing the tensile strength by the elastic modulus of concrete. Values plotted in Figure 6a were obtained by averaging the strain over a 8 mm wide strip of concrete centered with respect to the crack tip. The width of the strip was chosen considering the width of the FPZ in Figure 6b that shows the ε_{xx} at peak load for different values of *y*. It can be observed that the width of the FPZ can be roughly estimated to be in the range of 8-10 mm. From figure 6a, it is also possible to estimate the length, *c*, of the FPZ, i.e. the portion of the section where softening occurs. In most of the specimens, the value of *c* is comprised in the range 20-30 mm. From the experimental results, the value of *c* seems to vary with the specimen dimensions. This aspect will be further investigated in future studies.

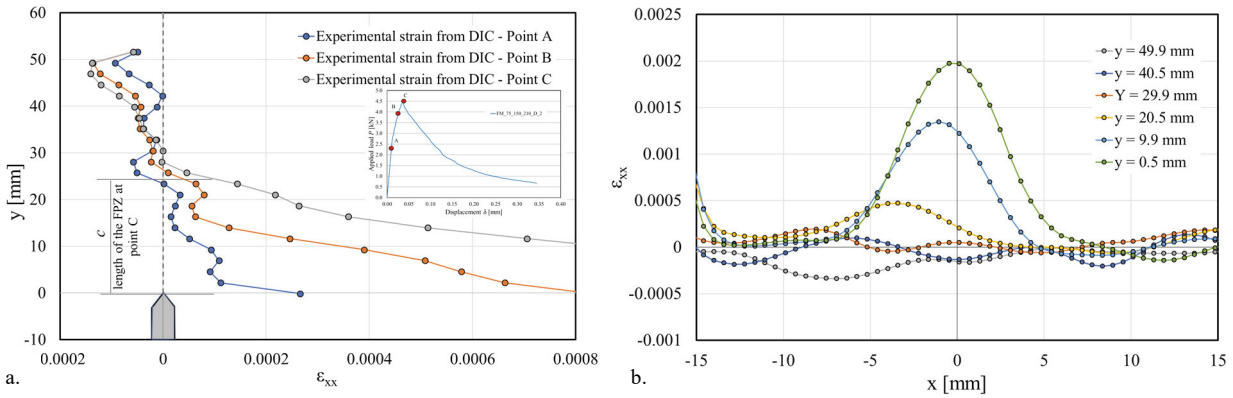

Fig. 6. *y*-ε_{xx} plot (a) and ε_{xx}-*x* plot (b) for specimen FM_75_150_210_D_2.

6. The lattice discrete particle model (LDPM)

Twenty numerical simulations were performed to conduct a preliminary investigation of the "width effect" through a numerical analysis. Simulations were performed using the lattice discrete particle model (LDPM), developed by Cusatis et al. (2011). The objective of the simulations was to capture some of the potential sources of the experimentally observed width effect, which are strain state across the ligament, wall-effect due to particle size and distribution. This preliminary study takes into account specimens with the same depth (150 mm) but with four different widths and were named following the notation FM_X_Y_N, where X indicates the specimen depth (*d*) in mm, Y represents the specimen width (*b*) in mm, and N = numerical simulation (Figure 7a). Concrete properties were calibrated simulating three-point bending tests on 150 mm depth × 150 mm width specimens and standard compressive tests on concrete cylinders in order to obtain a perfect match between the numerical results and the experimental ones. For each width, five tests were performed changing the distribution of the aggregates inside the concrete specimens.

Figure 7a shows the envelope of simulated load per unit width vs. CMOD curves for each width together with the average curve. The peak load per unit width increases when the specimen width decreases, as it was observed from experimental tests, even if the percentage increment in the peak value (4%) evaluated from the average curve among the larger and the smaller width is much smaller if compared with the one obtained from experimental results (22%) for 150 mm depth specimens. Observing the envelops in Figure 7a (dashed lines), the scatter of the numerical results seems to increase with decreasing widths. This scatter is particularly pronounced in 30 mm and 75 mm width specimens. Figure 7b shows the propagation of the crack at the peak load for a 150 mm width specimen. It can be observed that no damages are present close to the bottom steel supports.

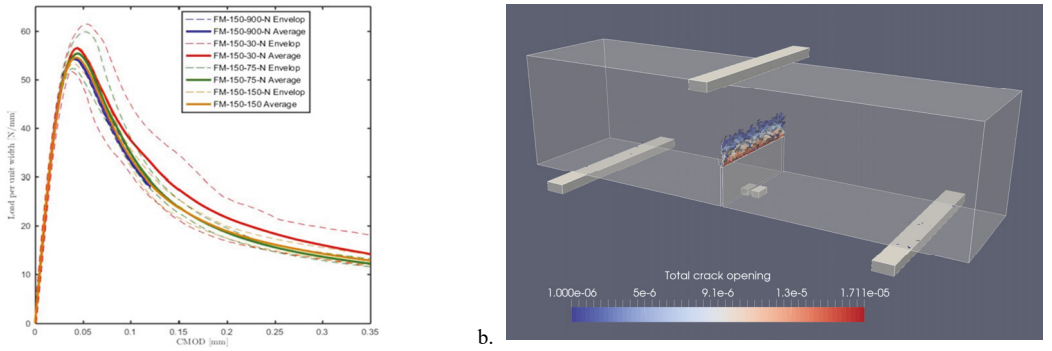

a. b.

Fig. 7. Load per unit width-CMOD responses from LDPM (a), propagation of the crack at peak load for a 150 mm width specimen (b).

Conclusions

The present study investigated through experimental tests and numerical simulation the effect of "width and size effect" on concrete notched prisms. Results show that the fracture energy of concrete, G_F, is almost size-independent, while G_f is affected by the size of the specimen. Experimental results show also a difference in the load per unit width peak value for specimens with different widths. Based on preliminary results of the numerical analysis the magnitude of the width effect cannot be confirmed.

Acknowledgements

The experimental work discussed in this paper was conducted at University of Bologna while numerical simulations were performed at BOKU University in Wien. Technicians of laboratory LISG (Laboratory of Structural and Geotechnical Engineering) at the University of Bologna are gratefully acknowledged for their help. The partial financial support by the Austrian Federal Ministry of Economy, Family and Youth and the National Foundation for Research, Technology and Development is gratefully acknowledged. The computational results presented have been achieved using the Vienna Scientific Cluster (VSC).

References

Bažant, Z. P., Oh, B. H., 1983. Crack band theory for fracture of concrete. Materials and structures, 16(3), 155-177.

Bazant, Z. P., Planas, J., 1997. Fracture and size effect in concrete and other quasibrittle materials (Vol. 16). CRC press.

British Standards Institution, 2004. Eurocode 2: Design of Concrete Structures: Part 1-1: General Rules and Rules for Buildings. British Standards Institution.

Carloni, C., 2014. Analyzing bond characteristics between composites and quasi-brittle substrates in the repair of bridges and other concrete structures. Advanced Composites in Bridge Construction and Repair, Woodhead Publishing Limited, Sawston, Cambridge, 61-93.

Elices, M., & Planas, J., 1996. Fracture mechanics parameters of concrete: an overview. Advanced Cement Based Materials, 4(3), 116-127.

Elices, M., Guinea, G. V., Planas, J. (1992). Measurement of the fracture energy using three-point bend tests: Part 3—influence of cutting the P-δ tail. Materials and Structures, 25(6), 327-334.

EN, B., 2009. 12390-3. Testing hardened concrete. Compressive strength of test specimens, 19.

EN, B., 2009. 12390-6. Testing Hardened Concrete. Tensile Splitting Strength of Test Specimens. British Standard Institution, London.

Gerstle, W., 2010. Progress in developing a standard fracture toughness test for concrete. In Structures Congress 2010 (pp. 1915-1926).

Hillerborg, A., 1985. Results of three comparative test series for determining the fracture energy G_F of concrete. Materials and Structures, 18(5), 407-413.

Hillerborg, A., 1985. The theoretical basis of a method to determine the fracture energy G_F of concrete. Materials and structures, 18(4), 291-296.

Hillerborg, A., Modéer, M., & Petersson, P. E., 1976. Analysis of crack formation and crack growth in concrete by means of fracture mechanics and finite elements. Cement and concrete research, 6(6), 773-781.

Kesler, C. E., Naus, D. J., & Lott, J. L., 1972. Fracture mechanics-its applicability to concrete. In Proceedings of the Society of Materials Science Conference on the Mechanical Behavior of Materials.

Petersson, P. E., 1981. Crack growth and development of fracture zones in plain concrete and similar materials. Division, Inst.

Planas, J., Elices, M., & Guinea, G. V. (1992). Measurement of the fracture energy using three-point bend tests: Part 2—Influence of bulk energy dissipation. Materials and Structures, 25(5), 305-312.

Walsh, P. F., 1976. Crack initiation in plain concrete. Magazine of Concrete Research, 28(94), 37-41.